Journal of Asian Earth Sciences 111 (2015) 100–112

Contents lists available at ScienceDirect

Journal of Asian Earth Sciences

journal homepage: www.elsevier.com/locate/jseaes

Geological, rare earth elemental and isotopic constraints on the origin of the Banbanqiao Zn–Pb deposit, southwest China

Bo Li [a,b,c], Jia-Xi Zhou [a,b,*], Zhi-Long Huang [a], Zai-Fei Yan [a], Guang-Ping Bao [a], Hai-Rui Sun [a]

[a] State Key Laboratory of Ore Deposit Geochemistry, Institute of Geochemistry, Chinese Academy of Sciences, Guiyang 550081, China
[b] Department of Land Resources Engineering, Kunming University of Science and Technology, Kunming 650093, China
[c] Kunming Prospecting Design Institute of China Nonferrous Metala Industry, Yunnan Copper Industry (Group) Co. Ltd., Kunming 650051, China

ARTICLE INFO

Article history:
Received 4 November 2014
Received in revised form 23 July 2015
Accepted 4 August 2015
Available online 4 August 2015

Keywords:
REE
C–O–S and Pb isotopes
Origin of hydrothermal fluids
The Banbanqiao Zn–Pb deposit
Western Yangtze Block
Southwest China

ABSTRACT

The newly discovered Banbanqiao Zn–Pb deposit in the southeastern part of the Sichuan–Yunnan–Guizhou (SYG) Pb–Zn metallogenic province is located on the western Yangtze Block, southwest China. Ore bodies of the Banbanqiao deposit are stratiform type, host in dolomitic limestone and dolostone of the Lower Carboniferous Dapu Formation and occur within the NNE-trending Banbanqiao anticline. More than 1.5 million tones (Mt) Zn–Pb ores at grades of 0.26–10.32 wt.% Pb and 0.81–28.8 wt.% Zn have been controlled until now. $\delta^{13}C_{PDB}$ and $\delta^{18}O_{SMOW}$ values of calcite separates range from −2.8‰ to −0.7‰ (average −1.1‰) and +14.1‰ to +17.0‰ (average +15.5‰), respectively. The $\delta^{13}C_{PDB}$ values are similar to those of marine carbonate rocks, but higher than those of mantle and significantly different from those of sedimentary organic matter. However, the $\delta^{18}O_{SMOW}$ values are among those of mantle, marine carbonate rocks and sedimentary organic matter. $\delta^{34}S_{CDT}$ values of sulfide separates range from +3.2‰ to +9.9‰ (average +6.5‰), unlike mantle-derived sulfur (0 ± 3‰), whilst lower than evaporites (+22‰ to +28‰) within host strata. $^{206}Pb/^{204}Pb$, $^{207}Pb/^{204}Pb$ and $^{208}Pb/^{204}Pb$ values of country shale and dolostone whole-rock samples are 18.47, 15.66 and 38.70, and 18.44–18.60, 15.66–15.85 and 38.70–39.14, respectively. Sulfide separates have $^{206}Pb/^{204}Pb$, $^{207}Pb/^{204}Pb$ and $^{208}Pb/^{204}Pb$ values ranging from 18.03 to 18.73, 15.65 to 15.78 and 38.15 to 39.14, respectively. These Pb isotopic data indicate a clearly crustal source of Pb in the plot of $^{207}Pb/^{204}Pb$ vs. $^{206}Pb/^{204}Pb$. Total REE (ΣREE) contents of country shale and dolostone whole-rock samples are 2.63 ppm and 0.72–86.2 ppm with δEu values are 2.79 and 0.34–0.70, respectively. Pyrite, sphalerite, galena and calcite samples have ΣREE contents of 5.3–36.4 ppm, 0.29–3.39 ppm, 0.52 ppm and 22.0–41.1 ppm, respectively, and δEu values of 0.64–0.86, 0.94–2.86, 0.32 and 0.21–0.45, respectively. These rare earth elemental and isotopic data suggest that the REE, C and S in the ore-forming fluids of the Banbanqiao deposit were mainly originated from the carbonate host rocks, while the Pb and O were primarily derived from radiogenic Pb- and ^{18}O-depleted sources, which are most likely to be the underlying Proterozoic basement rocks. Studies on the geology, rare earth elements and isotope geochemistry indicate that the Banbanqiao deposit is a carbonate-hosted, stratiform, anticline-controlled, epigenetic and high grade Zn–Pb deposit formed by elemental compositions of mixed origin, and is a typical SYG-type deposit in the western Yangtze Block, southwest China.

1. Introduction

The Sichuan–Yunnan–Guizhou (SYG) Pb–Zn metallogenic province contains 408 known Pb–Zn deposits with total more than 200 million tons Pb–Zn ores at average grade of 5 wt.% Pb and 10 wt.% Zn (Liu and Lin, 1999; Zhou et al., 2013a,b). Tectonically, this province is located on the western Yangtze Block, southwest China (Fig. 1A; Zheng and Wang, 1991; Cromie et al., 1996; Zhou et al., 2001; Han et al., 2007; Huang et al., 2010), where multiple orogenic events occurred (e.g., Zaw et al., 2007; Hu and Zhou, 2012; Pirajno, 2013). Studies have demonstrated that the Pb–Zn deposits in the SYG province have some similar features, including: (i) host in carbonate rocks of Sinian (Neoproterozoic Ediacaran) to Permian, (ii) occur within thrust fault and/or fold structures, (iii) high grade of Pb + Zn (>15 wt.%), (iv) spatially associated with the Permian Emeishan flood basalts (ca. ~260 Ma), and (v) ore bodies mainly formed at 222–192 Ma, much younger than the Emeishan basalts (e.g., Zheng and Wang, 1991; Liu and Lin, 1999;

* Corresponding author at: State Key Laboratory of Ore Deposit Geochemistry, Institute of Geochemistry, Chinese Academy of Sciences, Guiyang 550081, China.
E-mail address: zhoujiaxi@vip.gyig.ac.cn (J.-X. Zhou).

http://dx.doi.org/10.1016/j.jseaes.2015.08.007
1367-9120/

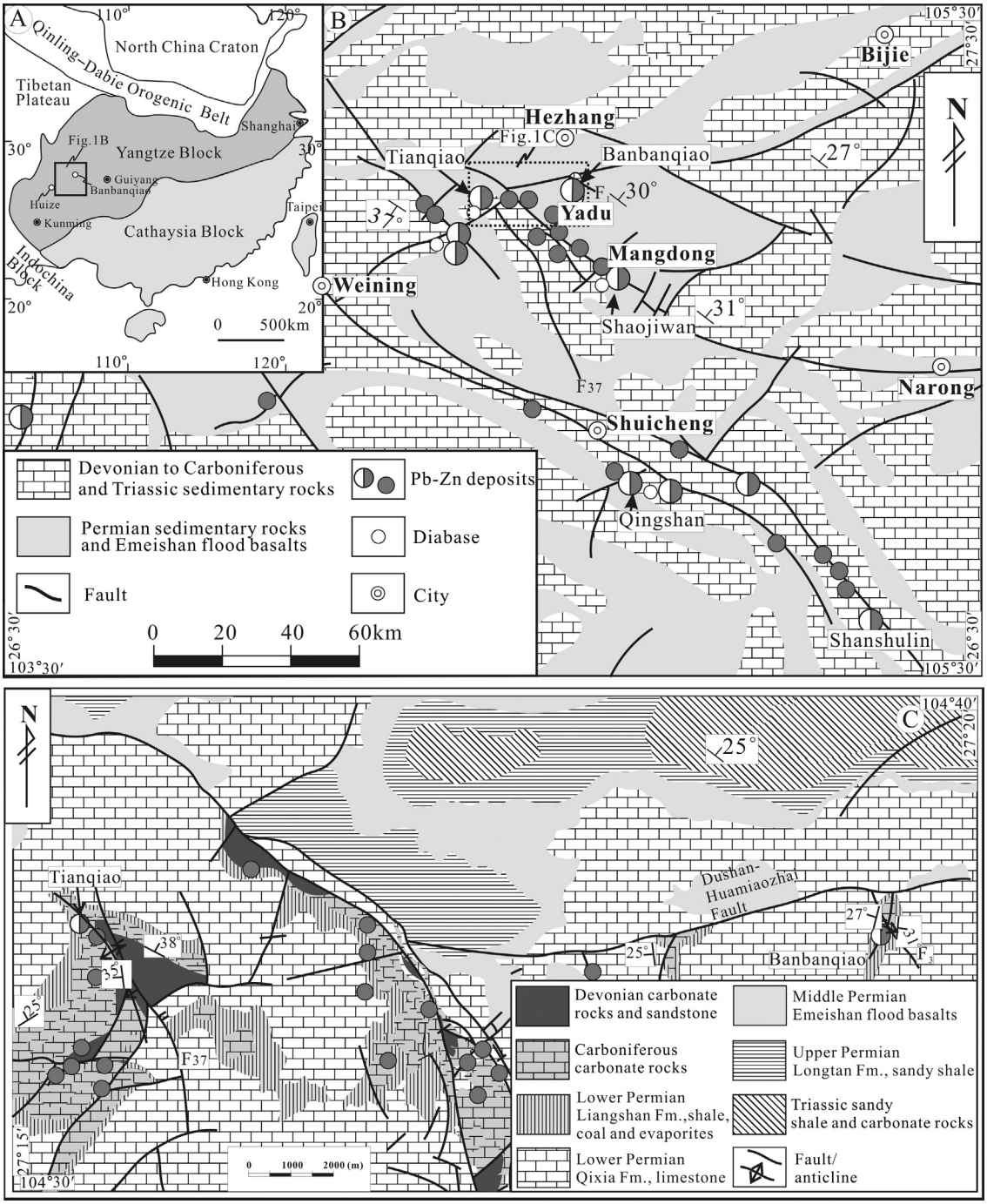

Fig. 1. (A) Tectonic setting map of South China. (B) Geological map of the southeastern Sichuan–Yunnan–Guizhou (SYG) Pb–Zn metallogenic province (after Zhou et al., 2013a). (C) Geological detailed map of the Tianqiao to Banbanqiao Pb–Zn ore fields (after Zhou et al., 2014a).

Deng et al., 2000; Hu and Zhou, 2012; Zhou et al., 2002a, 2013c,d, 2014a,b, 2015; Zhang et al., 2015). However, the sources of ore-forming elements and ore genesis of these Pb–Zn deposits in the SYG province have long been a matter of debate, although many research papers have published. For example, Chen (1986) considered that the elements were sourced from the carbonate host rocks, whereas Zhou et al. (2001) thought that the elements were derived from the Precambrian igneous rocks. Recently, Zhou et al. (2013a, 2014a, 2015) suggested that the Paleozoic ore-hosting carbonate rocks, Proterozoic basement rocks and Permian Emeishan flood basalts together provide the ore-forming elements for these deposits in the SYG province. On the other hand, although the most of these Pb–Zn deposits in the SYG province are clearly epigenetic, different opinions have been proposed on the ore genesis of them. These hypotheses include: (i) the Mississippi Valley-type (MVT) deposit related to basin brine (Zheng and Wang, 1991; Zhou et al., 2001; Wu et al., 2013; Zhang et al., 2015), (ii) the Permian Emeishan mantle plume-related deposit (Xie, 1963; Huang et al., 2003, 2010; Xu et al., 2014), and (iii) the unique SYG-type deposit that are different from the typical MVT deposit (Bai et al., 2013; Zhou et al., 2013a–c, 2014b). Recently, studies of Cd, Ge and Zn isotopes (Zhu et al., 2013; Zhou et al., 2014a,b; Meng et al., 2015), and *in situ* trace elements of sphalerite (Ye et al., 2011) have indicated that the ore genesis of these Pb–Zn deposits in the SYG province is

complex and cannot easily determined. Therefore, need more case studies to help us understanding the giant Pb–Zn mineralization in the SYG province.

The Banbanqiao deposit, a newly discovered Zn–Pb deposit, is located in the southeastern part of the SYG province (Zhou et al., 2014a). This deposit is not controlled by NW-trending regional ore-controlling structures (e.g. Yadu–Mangdong and Weining–Shuicheng) in northwest Guizhou province (Fig. 1A), but occurs within NNE-trending Banbanqiao anticline (Fig. 1B). We have reported some Zn–S and Pb isotopic data of the Banbanqiao deposit in previous study (Zhou et al., 2014a) and found that it has lower S and Pb isotopic values than those of the deposits occurred along the NW-trending regional faults (such as Shanshulin, Qingshan, Shaojiwan and Tianqiao) (Zhou et al., 2013a–c, 2014b), maybe represent different formation mechanism or ore-forming condition. Additionally, with the deepening of the exploration, we find that the Banbanqiao deposit has some other unique geological characteristics, including (i) hosts in carbonate rocks of Lower Carboniferous Dapu Formation, (ii) occurs as stratiform type within axis of Banbanqiao brachy anticline, (iii) the disseminated texture predominates, (iv) high Zn/(Zn + Pb) ratios (0.8–0.9), (v) simple mineralogy and weak wall rock alteration, and (vi) Lower Permian Liangshan Formation shale circle around (Figs. 1B and 2).

REE and C–O–S–Pb isotopes are powerful tools for tracing the source of the ore-forming elements (e.g., Zheng and Wang, 1991; Carr et al., 1995; Huston et al., 1995; Ohmoto and Goldhaber, 1997; Badrzadeh et al., 2011; Zhou et al., 2001, 2011, 2014a,b; Palinkaš et al., 2013; Pass et al., 2014). C–O–S and Pb isotopes have been widely used in previous studies for these Pb–Zn deposits in the SYG province (e.g., Zhou et al., 2001; Huang et al., 2003; Han et al., 2007; Li et al., 2007a; Zhou et al., 2013a, 2014a, 2015), whereas the studies of REE are limited (Huang et al., 2010; Zhou et al., 2011). Therefore, the Banbanqiao Zn–Pb deposit is used as case study in this paper, by analyzing REE contents of sulfide and calcite separates, and country shale and dolostone whole-rock samples, together with new C–O isotopic data and additional S–Pb isotopic data, the authors discuss the origin of the ore-forming elements, and propose a model that can account for the formation of Zn–Pb sulfide ores and provide new information for understanding the cause of a huge amount of base metals enriched in the SYG province.

2. Geological background

2.1. Regional geology

The Yangtze Block is composed of Archean to Proterozoic basement and Paleozoic to Mesozoic cover sequence (Liu and Lin, 1999; Zhou et al., 2002b). In the northern part of the Yangtze Block, sparse metamorphic rocks represent crystalline basement (Qiu et al., 2000; Hu and Zhou, 2012), whereas the Meso- to Neo-Proterozoic volcanic-sedimentary sequence represents folded basement in the western part (Yan et al., 2003; Sun et al., 2009; Zhao et al., 2010). The cover sequence of the western Yangtze Block consists mainly of Paleozoic and lower Mesozoic shallow marine sedimentary rocks, and Jurassic to Cenozoic terrestrial sediments (Liu and Lin, 1999; Yan et al., 2003; Huang et al., 2010). In the western Yangtze Block, the Permian mantle plume-derived Emeishan large igneous province (ca. ~260 Ma) covering an area of 250,000 km^2 (e.g., Chung and Jahn, 1995; Zhou et al., 2002b). This igneous province is dominantly composed of Emeishan flood basalts (Fig. 1B and C). During late Permian to early Jurassic, the western Yangtze Block collided with the Yidun arc resulting in the closure of the Paleo-Tethys Ocean. This event is known as the Indosinian (257–205 Ma) Orogeny (e.g., Han et al., 2007; Reid et al., 2007; Zhou et al., 2013a,d), and main thrust faults and folds in the western Yangtze Block related to it were affected by the later Yanshanian (205–65 Ma) and Himalayan (65–0 Ma) Orogeny (Zaw et al., 2007; Hu and Zhou, 2012; Pirajno, 2013).

More than 400 Pb–Zn deposits hosted in Neo-Proterozoic to Lower Permian carbonate rocks have been found in the western Yangtze Block (Liu and Lin, 1999). These deposits distribute in a large triangular area of 170,000 km^2 in SW Sichuan, NE Yunnan and NW Guizhou provinces (Zhou et al., 2013a; Xu et al., 2014; Zhang et al., 2015). This triangular area forms the famous SYG Pb–Zn metallogenic province (e.g., Liu and Lin, 1999; Zhou et al., 2001; Han et al., 2007; Huang et al., 2010; Zhou et al., 2013a, 2014a). Among these deposits, the Huize world-class Zn–Pb–Ge deposit (Fig. 1A) contains more than 5 Mt Zn–Pb metal reserves (Han et al., 2007; Zhou et al., 2013a). NS- and NE-trending faults are well developed in the western part of the SYG province (Liu and Lin, 1999; Han et al., 2007; Zhou et al., 2015), whereas NW-trending faults are dominant in the eastern part (Fig. 1B; Zhou et al., 2013a). It is obvious that these faults strictly control the distribution of Pb–Zn deposit in the SYG province (Fig. 1B and C; Han et al., 2007; Zhou et al., 2013b, 2014b, 2015; Zhang et al., 2015). Gypsum-bearing evaporites are widespread in the Cambrian to Triassic sedimentary rocks (Liu and Lin, 1999; Han et al., 2007) and are very important sulfur sources for the Pb–Zn deposits in the SYG province. The southeastern part of the SYG province, where the Banbanqiao deposit situated, has no Proterozoic basement rocks exposure and the cover sequence includes Devonian to Triassic sedimentary rocks (Fig. 1B) and the Permian Emeishan flood basalts (Fig. 1C). More than 100 Pb–Zn deposits have been found in this region, which hosted in dolomitic limestone and dolostone of Devonian to Lower Permian, and occurred along the main NW- and NE-striking structures (Fig. 1B and C). Most of the typical Pb–Zn deposits (such as Shanshulin, Qingshan, Shaojiwan and Tianqiao) in this region related to the NW-trending thrust faults and fold structures (Fig. 1B; Zhou et al., 2013e), whereas the newly found Banbanqiao Zn–Pb deposit situated in the NNE-trending fold structure (Figs. 1C and 2; Zhou et al., 2014a).

Geochronological studies in the SYG province have reported the calcite Sm–Nd isotopic ages of 222 ± 14 Ma (Li et al., 2007b) and 196 ± 13 Ma (Zhou et al., 2013d) for the Huize and Maozu deposits, respectively, and fluorite Sm–Nd age of 201.1 ± 2.9 Ma (Mao et al., 2012; Zhang et al., 2015) for the Jinshachang deposit. Sphalerite Rb–Sr ages for the Paoma, Tianqiao, Jinshachang and Lehong deposits are 200.1 ± 4.0 Ma (Lin et al., 2010), 191.9 ± 6.9 Ma (Zhou et al., 2013a), 206.8 ± 3.7 Ma (Zhou et al., 2015) and 200.9 ± 2.3 Ma (Mao et al., 2012). Thus, these typical Pb–Zn deposits in the SYG province formed at 222–192 Ma (Zhou et al., 2015).

2.2. Geology of the Banbanqiao ore deposit

2.2.1. Stratigraphy and lithology

In the Banbanqiao deposit area, the degree of geological work is relatively low in the past, with the deepening of the exploration, the strata were reclassified (Fig. 2). The Lower Carboniferous Dapu Formation was divided out from the previous decided Upper Carboniferous Huanglong-Maping Formation (Zhou et al., 2014a). Therefore, the exposed rocks include Lower Carboniferous Dapu Formation dolostone and dolomitic limestone, Upper Carboniferous Huanglong Formation dolostone and limestone. The Zn–Pb ore bodies of the Banbanqiao deposit are hosted by the dolomitic limestone and dolostone of the Lower Carboniferous Dapu Formation (Figs. 2 and 3). Overlying Carboniferous rocks are shale and coal of the Lower Permian Liangshan Formation, and limestone of Lower Permian Qixia Formation, all of which are overlain by the Middle Permian Emeishan basalts. Organic matter is widely distributed in the Lower Permian Liangshan Formation shale and coal.

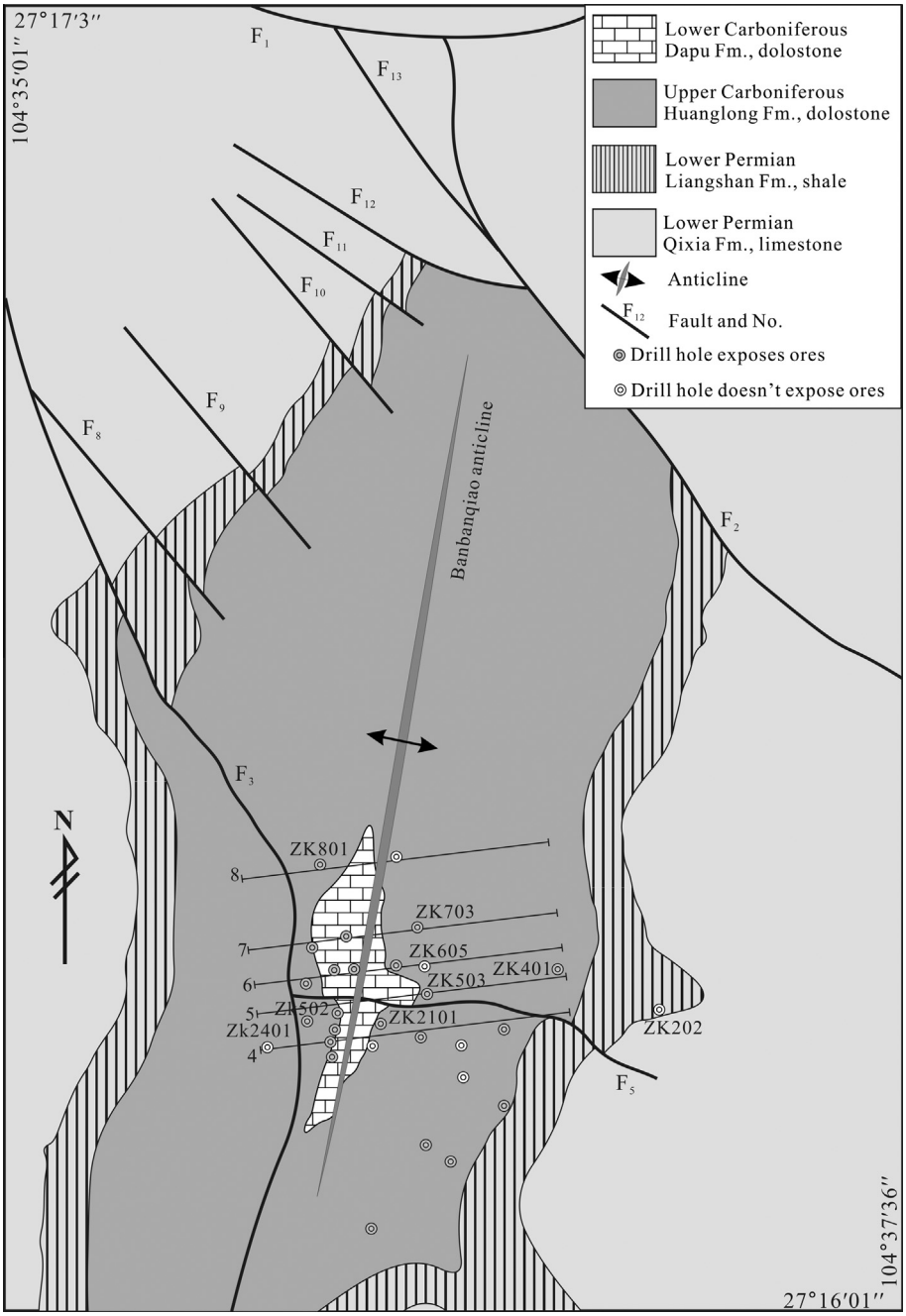

Fig. 2. Geological map of the Banbanqiao Zn–Pb deposit (after Zhou et al., 2014a).

2.2.2. Structure

Fault and fold structures in the Banbanqiao Zn–Pb deposit area are developed, including EW-trending Dushan-Huamianzhai thrust fault (F_1), series of NW-trending normal faults and NNE-trending Banbanqiao anticline (Figs. 1C, 2, and 3). The Dushan-Huamianzhai thrust fault (F_1) with dip angles between 40° and 70° is a regional structure that controls the distribution of Pb–Zn deposits in the studied area (Fig. 1B and C). In the Banbanqiao district, the NW-trending normal fault (F_3) has dip angles between 45° and 85°, and controls the occurrence of Zn–Pb ore bodies. The Lower Carboniferous Dapu Formation, Upper Carboniferous Huanglong Formation and Lower Permian Liangshan Formation strata form the Banbanqiao brachy anticline structure (Figs. 1C and 2). Ore bodies occur within axis of the Banbanqiao anticline (Fig. 3).

2.2.3. Ore body

Ore bodies in the Banbanqiao deposit are predominated by stratiform type (Fig. 3). There are three ore bodies have been found in the Banbanqiao deposit area, of which the No. II ore body is the largest. This ore body is stratiform, and occurs along the NW-trending normal fault (F_3) and within axis of the Banbanqiao brachy anticline (Fig. 3). Ore bodies in the Banbanqiao deposit contains more than 1.5 million tons Zn–Pb ores at grades of 0.26 wt.% to 10.32 wt.% Pb and 0.81 wt.% to 28.8 wt.% Zn, with high Zn/Pb ratios mostly

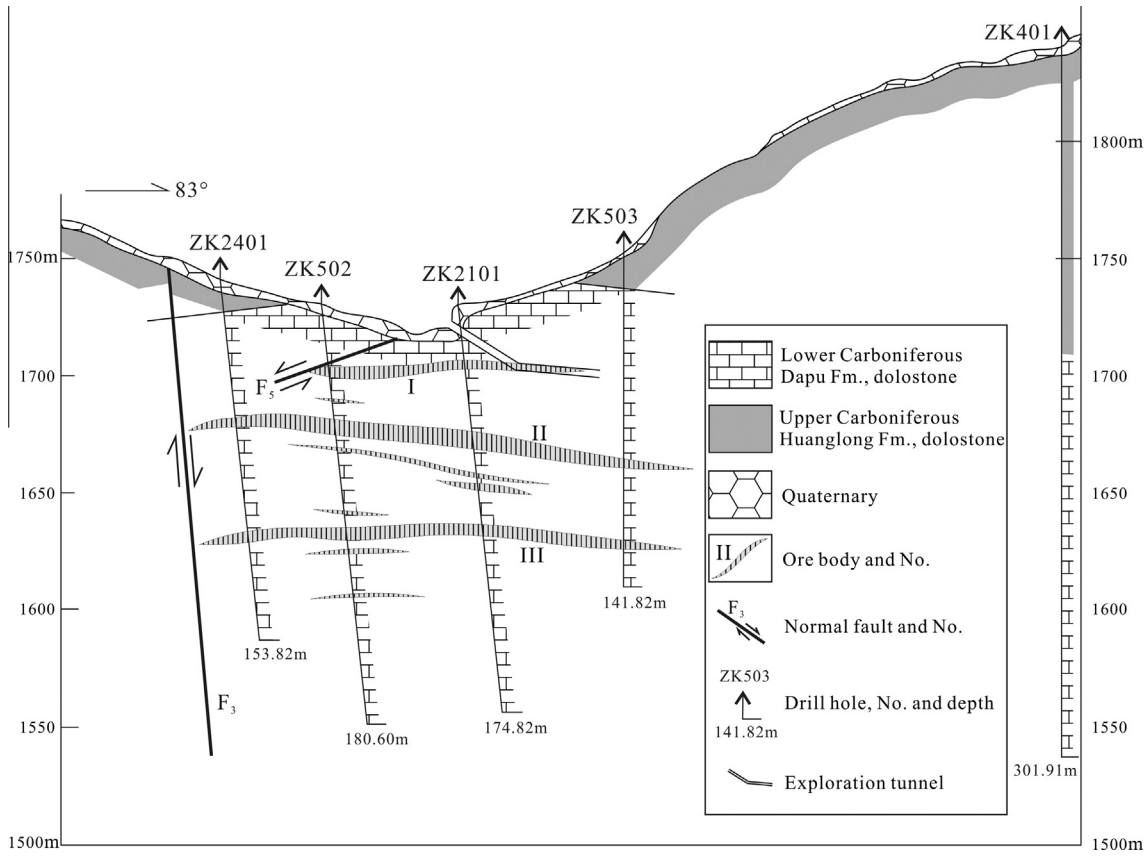

Fig. 3. Cross section of No. 5 exploration line in the Banbanqiao Pb–Zn deposit that shows shape of ore body, wall rocks and anticline (after Zhou et al., 2014a).

ranging from 4 to 12. Ores also contain major elements of S and Fe, and minor to trace elements of Cd, Ge and Ga (Zhou et al., 2014a).

2.2.4. Texture and structure of ores

Ores in the Banbanqiao Zn–Pb deposit underwent hydrothermal and supergene oxidizing processes (Zhou et al., 2014a). Therefore, there are oxidized and unaltered sulfide ores along with a mixture of these two types. Unaltered sulfide ores consist of sphalerite, pyrite, galena, calcite and dolomite. Oxidized and mixed ores have extremely complex mineral assemblages include smithsonite, limonite, cerussite, and sulfide and carbonate minerals. Within the unaltered sulfide ore zones, structures are composed of disseminated (Fig. 4A and E), massive (Fig. 4B and C), brecciated (Fig. 4D), vein (Fig. 4F) and banded, and textures consist of anhedral to euhedral granular (Fig. 5C, D, and F), metasomatic (Fig. 5A, B, and F), filling (Fig. 5D and E), and crush pressure shadows (Fig. 5D).

2.2.5. Mineral paragenesis

Based on crosscutting, overgrowth and replacement relationships, the hydrothermal period can be divided into two stages, including the sulfide–carbonate and the carbonate stages. In the sulfide–carbonate stage, the mineral assemblages include (i) pyrite + sphalerite + calcite (Fig. 4A, D, and F), (ii) pyrite + sphalerite + galena + calcite (Fig. 4C) and (iii) sphalerite + galena + calcite (Fig. 4B and E). Details about mineral paragenesis are listed in Table 1.

2.2.6. Wall rock alteration

Like other Pb–Zn deposits in the southeast SYG province, wall rock alteration types of the Banbanqiao Zn–Pb deposit are simple and mainly include: (i) dolomite, (ii) Fe–Mn carbonates, and (iii) zones of gossan consisting of iron and aluminum oxides and hydroxides. Dolomitization enhances rock brittleness and cause crack opening for Pb–Zn mineralization. Fe–Mn carbonatization resulted in light brown, maroon and puce Fe (Mn)-bearing dolomite and is closely associated with Pb–Zn mineralization. Gossan coexists with Pb–Zn sulfide ores on the space and is usually located in the upper levels of Pb–Zn mineralization zone. The Intensity of gossan formation is directly related to Pb–Zn mineralization (Zhou et al., 2014a).

3. Analytical methods

Fourteen representative sulfide ore hand specimens from drill holes and exploration tunnels were collected. Pyrite, sphalerite, galena and calcite were hand picked from these samples using a binocular microscope and analyzed for REE, and C, O, S and Pb isotopes. Additionally, one whole-rock sample of Lower Permian Liangshan Formation shale and eight whole-rock samples of Lower Carboniferous Dapu Formation dolostone were collected for REE and Pb isotopes.

3.1. Carbon and Oxygen isotope analysis

C and O isotopes' analysis was completed at the State Key Laboratory of Environmental Geochemistry, Chinese Academy of Sciences, by using a Finnigan MAT-253 mass spectrometer. Calcite reacts with 100% phosphoric acid (H_3PO_4) to produce CO_2. The analytical precisions ($2\sigma_m$) are ±0.3‰ for $\delta^{13}C$ value and ±0.6‰ for $\delta^{18}O$ value. C and O isotopic compositions are reported relative to Vienna Pee Dee Belemnite (V-PDB). $\delta^{18}O_{SMOW} = 1.03086 \times \delta^{18}O_{PDB} + 30.86$ (Friedman and O'Neil, 1977).

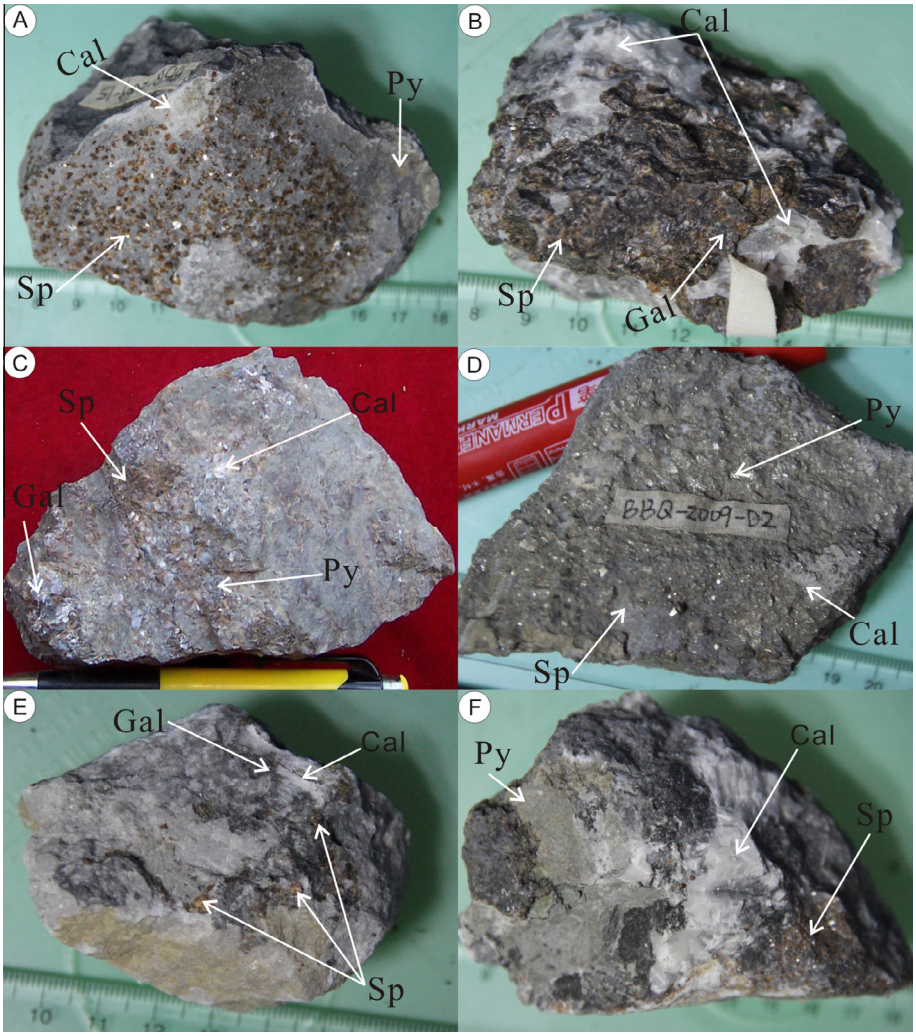

Fig. 4. Photos of ore types and mineral assemblages in the Banbanqiao deposit. (A) Euhedral granular sphalerite (Sp) with massive pyrite (Py) and patchy calcite (Cal). (B) Patchy and vein Cal with massive Sp and granular galena (Gal). (C) Massive and veined Sp with granular pyrite and patchy Cal. (D) Euhedral granular Py with massive Sp and patchy Cal. (E) Granular Sp with patchy Cal and fine-grained Gal. (F) Vein Cal with massive Sp and Py.

3.2. Sulfur isotope analysis

Sulfur isotopes' analysis was carried out by using the Element Analyzer (EA) method on a Continuous Flow Isotope Ratio Mass Spectrometry at the State Key Laboratory of Environment Geochemistry, Chinese Academy of Sciences. GBW 04415 and GBW 04414 Ag_2S were used as the external standards and Vienna Canyon Diablo Troilite (V-CDT) was the referent standard. Analytical accuracy is ±0.2‰ ($2\sigma_m$).

3.3. Lead isotope analysis

Pb isotopes' analysis was carried out using the GV IsoProbe-T thermal ionization mass spectrometer (TIMS) at the Beijing Institute of Uranium Geology. The analytical procedures involved dissolution of samples using HF and $HClO_4$ in crucibles, followed by basic anion exchange resin to purify the Pb. Analytical results for the standard NBS 981 are $^{208}Pb/^{206}Pb = 36.612 \pm 0.005$ ($2\sigma_m$), $^{207}Pb/^{206}Pb = 15.458 \pm 0.004$ ($2\sigma_m$) and $^{206}Pb/^{204}Pb = 16.935 \pm 0.003$ ($2\sigma_m$).

3.4. REE analysis

Dissolution of sulfide and calcite separates, and shale and dolostone whole-rock samples was completed in the State Key Laboratory of Ore Deposit Geochemistry, Chinese Academy of Sciences, and then REE contents of sulfide separates were analyzed using an ELAN DRC-e ICP-MS at the Beijing Institute of Uranium Geology, and calcite separates and whole-rock samples were analyzed using an ELAN DRC-e Q-ICP-MS, at the State Key Laboratory of Ore Deposit Geochemistry, Chinese Academy of Sciences. A detailed analytical procedure for REE analysis is available in Qi et al. (2000). Relative analytical error for REE is better than 5% ($2\sigma_m$).

4. Analytical results

4.1. Carbon and Oxygen isotopic compositions

C–O isotopic compositions of calcite separates from sulfide ore samples are listed in Table 2 and plotted in Fig. 6. The $\delta^{13}C_{PDB}$ and $\delta^{18}O_{SMOW}$ values of nine calcite separates range from −2.8‰ to −0.7‰ (mean −1.1‰) and +14.1‰ to +17.0‰ (mean +15.5‰), respectively. Compared with the well-known Huize (Huang et al., 2010) and Tianqiao (Zhou et al., 2013a) deposits in the SYG province, calcite separates from the Banbanqiao deposit have higher $\delta^{13}C_{PDB}$ values, but lower $\delta^{18}O_{SMOW}$ values (Fig. 6).

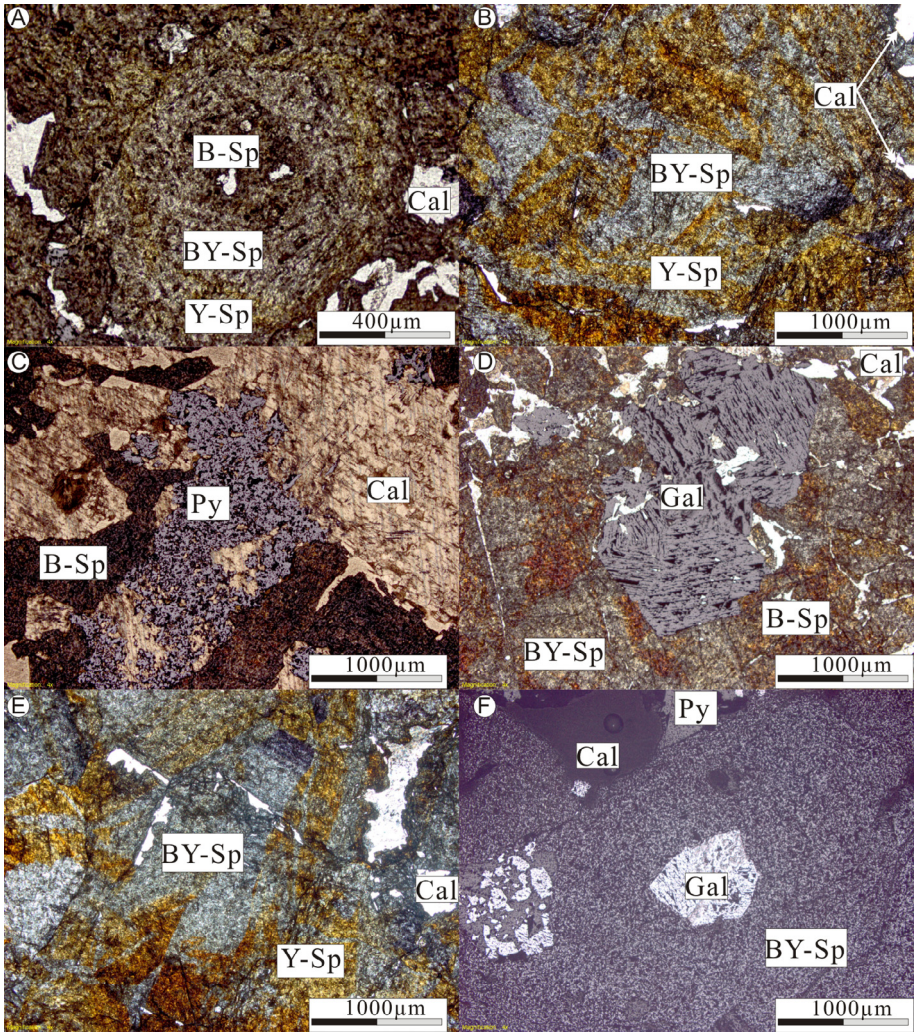

Fig. 5. Photos of microscopic structures for sulfide ores in the Banbanqiao deposit. (A) Patchy calcite (Cal) within brown sphalerite (B-Sp), and B-Sp within brown–yellow sphalerite (BY-Sp), which enclosed in yellow sphalerite (Y-Sp). (B) BY-Sp enclosed in Y-Sp within. (C) B-Sp with pyrite (Py) and Cal. (D) Early Cal enclosed in galena (Gal) and BY-SP, and Gal within B-Sp and BY-Sp. (E) Cal within Gal and BY-Sp, and BY-Sp enclosed in Y-Sp. (F) Gal within BY-Sp, and BY-Sp coexisting with Cal and Py. (For interpretation of the references to colour in this figure legend, the reader is referred to the web version of this article.)

Table 1
Mineral paragenesis in the Banbanqiao deposit.

Period	Hydrothermal				Supergene
Stage	Sulfide–carbonate			Carbonate	Oxidized
Mineral assemblage	Sp + Py + Cal	Sp + Py + Gal + Cal	Sp + Gal + Cal	Dol + Cal	Lim + Cer
Sp	▬	▬	▬		
Py	▬	▬	—		
Gal	—	▬	▬		
Dol	—	—	—	▬	
Cal	▬	▬	▬	▬	
Lim					▬
Cer					▬

Sp, sphalerite; Py, pyrite; Gal, galena; Cal, calcite; Dol, dolomite; Lim, limonite; Cer, Cerussite. — Less; ▬ More.

4.2. Sulfur isotopic compositions

$\delta^{34}S_{CDT}$ values of sulfide separates from sulfide ore samples are shown in Table 3 and plotted in Fig. 7. All sulfide separates have $\delta^{34}S_{CDT}$ values ranging from +3.2‰ to +9.9‰ (mean +6.5‰, $n = 21$), of which pyrite, sphalerite and galena samples have $\delta^{34}S_{CDT}$ values ranging from +8.8‰ to +9.9‰ (mean +9.5‰, $n = 5$), +3.9‰ to +9.0‰ (mean +6.4‰, $n = 11$), and +3.2‰ to +4.8‰ (mean +3.9‰, $n = 5$), respectively. It is clear that from pyrite to sphalerite, and then to galena, the $\delta^{34}S_{CDT}$ values are decreasing, reflecting sulfur isotope equilibrium fractionation. Sulfide separates from the Banbanqiao deposit have lower $\delta^{34}S_{CDT}$ values (Fig. 7) than those of the Tianqiao (Zhou et al., 2013a), Shaojiwan (Zhou et al., 2013b), Qingshan (Zhou et al., 2013c) and Shanshulin

Table 2
C–O isotopic compositions of calcite separate.

No.	Object	$\delta^{13}C_{PDB}$/‰	$2\sigma_m$	$\delta^{18}O_{PDB}$/‰	$2\sigma_m$	$\delta^{18}O_{SMOW}$/‰	$\delta^{18}O_{H2O}$/‰
B06	Calcite	−1.2	0.1	−14.1	0.2	+16.3	+6.8
B08	Calcite	−2.8	0.2	−13.5	0.2	+17.0	+7.5
B09	Calcite	−1.2	0.2	−14.1	0.2	+16.3	+6.8
B10	Calcite	−0.8	0.1	−16.0	0.2	+14.4	+4.9
B15	Calcite	−0.8	0.1	−15.1	0.1	+15.3	+5.8
B17	Calcite	−1.0	0.1	−14.8	0.2	+15.6	+6.1
B18	Calcite	−0.7	0.1	−14.1	0.2	+16.3	+6.8
B21	Calcite	−0.7	0.1	−16.3	0.1	+14.1	+4.6
B924	Calcite	−0.8	0.1	−16.0	0.2	+14.4	+4.9

$\delta^{18}O_{SMOW} = 1.03086 \times \delta^{18}O_{PDB} + 30.86$ (Friedman and O'Neil, 1977); $\Delta^{18}O_{Cal\text{-}H2O} = \delta^{18}O_{Cal} - \delta^{18}S_{H2O} = 2.78 \times 10^6/(t + 273.15)^2 - 2.89$, $t = 200$ °C (Zheng and Chen, 2000).

(Zhou et al., 2014b) deposits in the southeastern part of the SYG province (Fig. 1B), whereas similar to those of the Huize deposit in the central part of the SYG province (Fig. 1A; Han et al., 2007).

4.3. Lead isotopic compositions

Lead isotopic compositions of whole-rock and sulfide separate samples are listed in Table 4 and shown in Fig. 8. Twelve sulfide separate samples have $^{206}Pb/^{204}Pb$ ratios between 18.029 and 18.726 (average 18.283), $^{207}Pb/^{204}Pb$ rations between 15.651 and 15.784 (average 15.687) and $^{208}Pb/^{204}Pb$ ratios between 38.145 and 39.138 (average 38.425). The $^{238}U/^{204}Pb$ (μ) values range from 9.60 to 9.81 (average 9.65). Eight dolostone whole-rock samples have $^{206}Pb/^{204}Pb$ ratios ranging from 18.436 to 18.602 (average 18.519), $^{207}Pb/^{204}Pb$ ratios ranging from 15.663 to 15.850 (average 15.754) and $^{208}Pb/^{204}Pb$ ratios ranging from 38.703 to 39.140 (average 38.842). The μ values range from 9.58 to 9.94 (average 9.76). One shale whole-rock sample has $^{206}Pb/^{204}Pb$, $^{207}Pb/^{204}Pb$ and $^{208}Pb/^{204}Pb$ ratio of 18.467, 15.656 and 38.704. The μ value is 9.57. It is obvious that most sulfide samples have lower radiogenic Pb than those of country whole-rock (Fig. 8A and B).

4.4. REE contents

REE contents of country whole-rock, sulfide and calcite separate samples are listed in Table 5 and shown in Fig. 9. One shale whole-rock sample has total REE (ΣREE, excluding Y) content of 2.63 ppm, δEu value of 2.79 and La/Yb_N ratio of 2.86. Eight dolostone whole-rock samples have (i) total REE contents ranging from 0.72 ppm to 86.2 ppm (average 27.4 ppm), (ii) δEu values ranging from 0.34 to 0.70 (average 0.56), and (iii) La/Yb_N ratios ranging from 1.92 to 6.76 (average 4.70). Twelve sulfide separate samples have ΣREE contents ranging from 0.29 ppm to 36.4 ppm (average 4.27 ppm), δEu values ranging from 0.32 to 2.86 (average 1.72) and La/Yb_N ratios ranging from 0.4 to 27.24 (average 7.46). These sulfide samples are distinguished by: (i) two pyrite separates have ΣREE contents ranging from 5.27 ppm to 36.4 ppm, δEu values between 0.64 and 0.86 and La/Yb_N ratios of 1.67–10.49, (ii) nine sphalerite separates have ΣREE contents ranging from 0.39 to 3.39 ppm, δEu values ranging from 0.94 to 2.86 and La/Yb_N ratios ranging from 0.4 to 12.26, and (iii) one galena separate has ΣREE content of 0.52 ppm, δEu value of 0.32 and La/Yb_N ratio of 27.24. Two calcite separate have ΣREE contents ranging from 22.0 to 41.1 ppm, δEu values between 0.21 and 0.45 and La/Yb_N ratios of 5.54–8.42. Obviously, calcite and pyrite separates have higher REE contents than those of sphalerite and galena. In addition, it is clear that the pyrite, calcite and galena separates have negative Eu anomaly, whereas almost all the sphalerite separates have positive Eu anomaly.

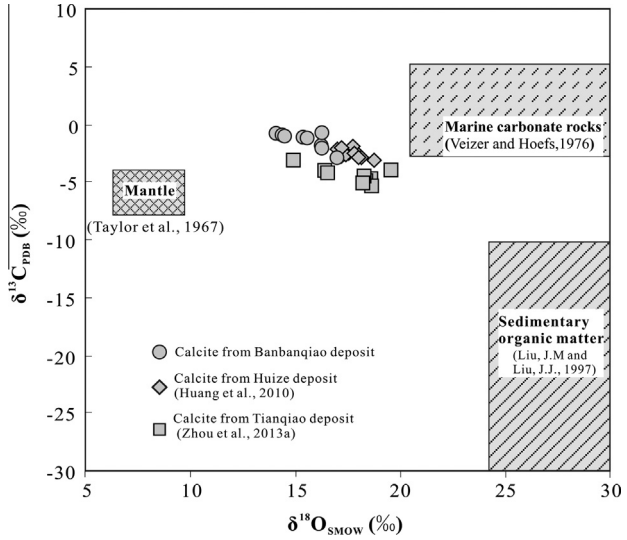

Fig. 6. Plot of $\delta^{13}C_{PDB}$ vs. $\delta^{18}O_{SMOW}$ values. The $\delta^{13}C_{PDB}$ and $\delta^{18}O_{SMOW}$ values for calcite separates from the Banbanqiao deposit compared with mantle, marine carbonate rocks and sedimentary organic matter, and those from the Huize and Tianqiao deposits.

5. Discussions

5.1. Origin of ore-forming elements

5.1.1. Constraints from C–O isotopes

Generally, there are three principal sources of C in hydrothermal fluids: (i) mantle, (ii) marine carbonate rocks, and (iii) sedimentary organic matter (Taylor et al., 1967; Veizer and Hoefs, 1976; Demény and Harangi, 1996; Liu and Liu, 1997; Demény et al., 1998). The $\delta^{13}C_{PDB}$ values for mantle, marine carbonate and

Table 3
Sulfur isotopic compositions of sulfide separate.

No.	$\delta^{34}S_{CDT}$/‰ ($2\sigma_m$)			T (°C)
	Pyrite	Sphalerite	Galena	
B02	+8.8 ± 0.1	+5.7 ± 0.1		
B04		+6.2 ± 0.2	+3.2 ± 0.1	224
B06	+9.8 ± 0.2			
B08		+8.4 ± 0.1	+4.5 ± 0.1	163
B09	+9.6 ± 0.1	+6.4 ± 0.1		
B10		+6.0 ± 0.1	+3.5 ± 0.1	271
B15		+3.9 ± 0.2		
B17		+6.1 ± 0.1	+3.6 ± 0.2	271
B18	+9.2 ± 0.2	+6.6 ± 0.2		
B20		+4.8 ± 0.2		
B21		+9.0 ± 0.1	+4.8 ± 0.1	147

$\Delta^{34}S_{Sp\text{-}Gal} = \delta^{34}S_{Sp} - \delta^{34}S_{Gal} = 0.74 \times 10^6/(t + 273.15)^2$ (Czamanske and Rye, 1974).

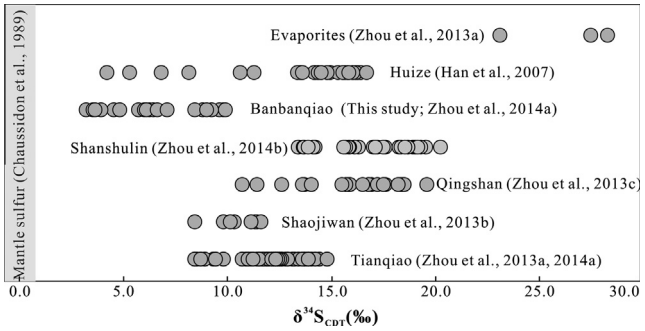

Fig. 7. Sulfur isotopic compositions histogram for the Banbanqiao deposit. The $\delta^{34}S_{CDT}$ values for the Banbanqiao deposit compared with mantle-derived sulfur and evaporites, and the Huize, Tianqiao, Shaojiwan, Qingshan and Shanshulin deposits in the SYG province.

organic matter range from −4.0‰ to −8.0‰ (Taylor et al., 1967), −4.0‰ to +4.0‰ (Veizer and Hoefs, 1976), and −30.0‰ to −10.0‰ (Liu and Liu, 1997), respectively. Calcite separates from the Banbanqiao deposit have $\delta^{13}C_{PDB}$ values higher than those of mantle and organic matters, but similar to those of marine carbonate (Fig. 6). This indicates that mantle and organic matter did not contribute significant quantities of C to the hydrothermal fluids, and so the C in the ore-forming fluids was likely provided by the carbonate host rocks, similar to other carbonate-hosted Pb–Zn deposits in the studied region (Zhou et al., 2013a, 2014b, 2015). The $\delta^{18}O_{SMOW}$ values of calcite separates from the Banbanqiao deposit are higher than those of mantle (+6.0‰ to +10.0‰; Taylor et al., 1967), but lower than those of marine carbonate rocks ($\delta^{18}O_{SMOW}$ = +20.0‰ to +30.0‰; Veizer and Hoefs, 1976) and sedimentary organic matter ($\delta^{18}O_{SMOW}$ = +24.0‰ to +35.0‰; Liu and Liu, 1997). The calculated $\delta^{18}O_{H2O}$ values of the hydrothermal fluids range from +4.6‰ to +7.5‰ based on oxygen isotope equilibrium fractionation equation between calcite and water ($\Delta^{18}O_{Cal\text{-}H2O} = \delta^{18}O_{Cal} - \delta^{18}S_{H2O} = 2.78 \times 10^6/(t + 273.15)^2 - 2.89$, t = 200 °C; Zheng and Chen, 2000), which are similar to those of mantle-derived O (Demény and Harangi, 1996; Demény et al., 1998). In the plot of $\delta^{13}C_{PDB}$ vs. $\delta^{18}O_{SMOW}$ values (Fig. 5A), all calcite separates from the Banbanqiao deposit plotted in the field between mantle and marine carbonate rocks, but away from those of sedimentary organic matter. These suggest that the ore-forming fluids were ^{18}O-depleted compared with the carbonate host rocks and were likely to be derived from a mixed source region (the mantle-derived O in Emeishan basalts and dissolved O from the carbonate host rocks). Calcite separates from the Huize (Huang et al., 2010) and Tianqiao (Zhou et al., 2013a) deposits have $\delta^{13}C_{PDB}$ values lower than those of the Banbanqiao deposit suggests more C in the formers were derived from mantle (Huang et al., 2010) and/or organic material (Zhou et al., 2013a).

Table 4
Pb isotopic compositions of country whole-rock and sulfide separate.

No.	Object	$^{206}Pb/^{204}Pb$[a] ($2\sigma_m$)	$^{207}Pb/^{204}Pb$[a] ($2\sigma_m$)	$^{208}Pb/^{204}Pb$[a] ($2\sigma_m$)	μ[b]
B903	Shale	18.467 ± 0.002	15.656 ± 0.003	38.704 ± 0.004	9.57
B904	Dolostone	18.436 ± 0.004	15.675 ± 0.002	38.736 ± 0.005	9.61
B905	Dolostone	18.558 ± 0.005	15.763 ± 0.003	39.030 ± 0.007	9.77
B908	Dolostone	18.497 ± 0.003	15.663 ± 0.002	38.735 ± 0.006	9.58
B912	Dolostone	18.551 ± 0.002	15.850 ± 0.003	38.756 ± 0.005	9.94
B913	Dolostone	18.602 ± 0.002	15.748 ± 0.002	38.703 ± 0.006	9.73
B920	Dolostone	18.517 ± 0.002	15.735 ± 0.003	38.913 ± 0.004	9.72
B923	Dolostone	18.509 ± 0.002	15.816 ± 0.003	39.140 ± 0.006	9.88
B925	Dolostone	18.483 ± 0.002	15.782 ± 0.003	38.720 ± 0.005	9.82
B03	Pyrite	18.571 ± 0.001	15.689 ± 0.001	38.675 ± 0.003	9.62
B06	Pyrite	18.280 ± 0.001	15.705 ± 0.001	38.609 ± 0.002	9.69
B05	Sphalerite	18.130 ± 0.001	15.651 ± 0.002	38.145 ± 0.002	9.64
B08	Sphalerite	18.200 ± 0.001	15.665 ± 0.001	38.261 ± 0.002	9.63
B09	Sphalerite	18.153 ± 0.002	15.674 ± 0.001	38.229 ± 0.001	9.69
B15	Sphalerite	18.133 ± 0.001	15.658 ± 0.001	38.161 ± 0.001	9.61
B17	Sphalerite	18.270 ± 0.001	15.676 ± 0.002	38.393 ± 0.002	9.62
B18	Sphalerite	18.176 ± 0.002	15.668 ± 0.001	38.201 ± 0.002	9.60
B20	Sphalerite	18.726 ± 0.001	15.715 ± 0.001	38.850 ± 0.003	9.62
B21	Sphalerite	18.029 ± 0.001	15.656 ± 0.002	38.154 ± 0.001	9.63
B924	Sphalerite	18.159 ± 0.001	15.701 ± 0.001	38.286 ± 0.003	9.66
B10	Galena	18.564 ± 0.002	15.784 ± 0.003	39.138 ± 0.007	9.81

[a] Age-corrected (200 Ma).
[b] $\mu = {}^{238}U/{}^{204}Pb$.

5.1.2. Implications from S isotopes

Sulfide ores in the Banbanqiao deposit have simple sulfur-bearing minerals assemblage of galena, sphalerite and pyrite, but lack sulfate (Zhou et al., 2014a). Since sulfate minerals are not present in the Banbanqiao deposit, the equilibrium–disequilibrium constraints between sulfide minerals pairs such as pyrite–sphalerite and sphalerite–galena that deposited contemporaneously have the most significance. The $\delta^{34}S$ values' differences between nine sulfide minerals pairs from the same hand specimen ranging +2.5‰ to +4.2‰, and the relations of $\delta^{34}S_{pyrite} > \delta^{34}S_{sphalerite}$ and $\delta^{34}S_{sphalerite} > \delta^{34}S_{galena}$ for these pairs suggests that sulfide precipitated under sulfur isotope equilibrium fractionation. The observed fractionation for five sphalerite–galena pairs in the Banbanqiao Zn–Pb deposit corresponds to mineral formation temperatures (Czamanske and Rye, 1974) of 147–271 °C (Table 3). Studies have demonstrated that in low oxidation state sulfur isotopic compositions of sulfide minerals (especially pyrite) approximately represent the $\delta^{34}S$ values of the hydrothermal fluids (e.g., Ohmoto, 1972; Ohmoto et al., 1990; Dixon and Davidson, 1996; Seal, 2006; Basuki et al., 2008; Pass et al., 2014). Pyrite from the Banbanqiao deposit has $\delta^{34}S_{CDT}$ values ranging from +8.8‰ to +9.9‰ (mean +9.5‰), unlike mantle-derived sulfur (0 ± 3‰; Chaussidon et al., 1989). Sulfate-bearing evaporites in Permian strata (Fig. 7) have $\delta^{34}S_{CDT}$ values ranging from +22‰ to +28‰ (Zhou et al., 2014a), within the range of Cambrian to Triassic seawater (+15‰ to +35‰; Claypool et al., 1980). Thermal chemical reduction of sulfate to sulfide can lower $\delta^{34}S$ values up to +15‰ (e.g., Ohmoto et al., 1990; Ohmoto and Goldhaber, 1997; Basuki et al., 2008; Pass et al., 2014) such that the reduced sulfur in sulfide ores interpreted to be the produces of evaporites within the Permian strata by thermal chemical sulfate reduction (TSR). The metallogenic temperatures range from 147 °C to 271 °C (Table 3), excluding bacterial sulfate reduction, which would result in a larger sulfur isotope fractionation. Therefore, S in the hydrothermal fluids was mainly sourced from evaporites by TSR with a limited influence of mantle-derived S as suggested by O isotopic data above.

5.1.3. Constrained by Pb isotopes

Because some Pb isotopes are radiogenic, the Pb isotopic ratios need to be corrected to a consistent age in order to make comparisons between different phases. Sulfides have very low U and Th contents, hence the radiogenic Pb of sulfides after their formation is negligible and no age correction is needed, whereas the Pb isotopes in the whole-rock are needed. (e.g., Carr et al., 1995; Muchez et al., 2005; Pass et al., 2014; Zhou et al., 2014b). Previous studies have demonstrated that these typical Pb–Zn deposits in the SYG province formed at ~200 Ma, which is used for correcting the Pb isotope of whole-rock. In the diagram of $^{207}Pb/^{204}Pb$ vs. $^{206}Pb/^{204}Pb$ ratios (Fig. 8A), all the sulfides and country whole-rock samples plot in the upper crust lead average evolution curve (Zartman and Doe, 1981). In the plot of $^{208}Pb/^{204}Pb$ vs. $^{206}Pb/^{204}Pb$ ratios (Fig. 8B), they are plotted near to the orogenic belt lead average evolution curve (Zartman and

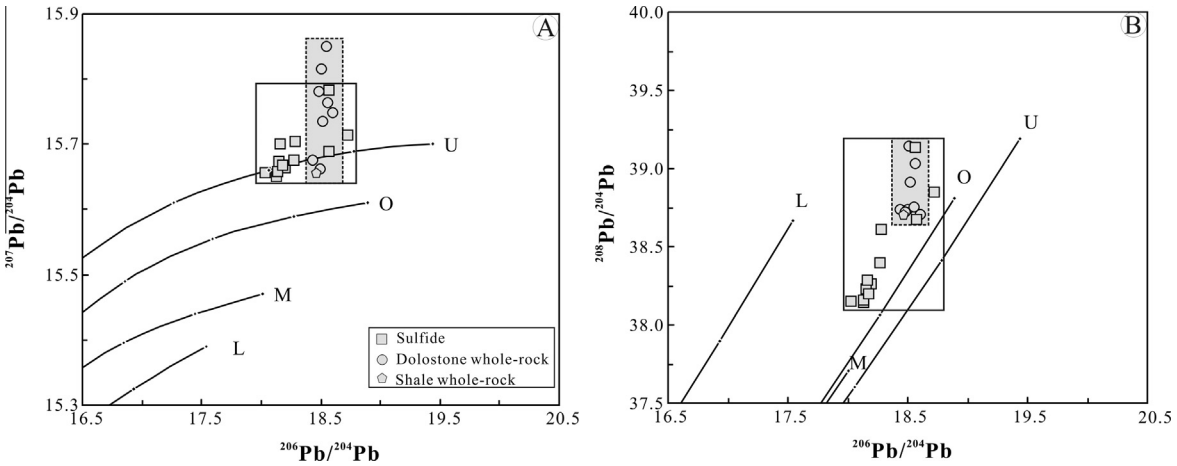

Fig. 8. Plots of $^{207}Pb/^{204}Pb$ vs. $^{206}Pb/^{204}Pb$ (A) and $^{208}Pb/^{204}Pb$ vs. $^{206}Pb/^{204}Pb$ (B) ratios for sulfides and wall rocks. Trends for the Upper Crust (U), Orogen belt (O), Mantle (M) and Lower Crust (L) are taken from Zartman and Doe (1981).

Table 5
REE contents (ppm) of country whole-rock, and sulfide and calcite separate.

No.	Object	La	Ce	Pr	Nd	Sm	Eu	Gd	Tb	Dy	Ho	Er	Tm	Yb	Lu	ΣREE	δEu	$(La/Yb)_N$
B903	Shale	0.424	0.773	0.093	0.445	0.102	0.124	0.180	0.027	0.163	0.039	0.126	0.018	0.100	0.017	2.63	2.79	2.86
B904	Dolostone	10.1	14.9	2.16	8.09	1.58	0.357	1.89	0.263	1.49	0.340	1.02	0.159	1.070	0.165	43.6	0.63	6.36
B905	Dolostone	0.384	0.457	0.079	0.346	0.065	0.017	0.088	0.018	0.105	0.026	0.073	0.011	0.076	0.014	1.76	0.68	3.43
B908	Dolostone	3.41	4.90	0.689	3.14	0.784	0.172	1.054	0.147	0.828	0.188	0.442	0.063	0.340	0.052	16.2	0.58	6.76
B912	Dolostone	0.711	0.774	0.124	0.471	0.111	0.028	0.167	0.026	0.159	0.034	0.097	0.013	0.075	0.011	2.80	0.63	6.43
B913	Dolostone	0.954	0.954	0.147	0.601	0.145	0.030	0.216	0.034	0.196	0.048	0.143	0.022	0.110	0.021	3.62	0.51	5.85
B923	Dolostone	14.7	25.9	2.56	7.54	1.14	0.208	2.20	0.307	2.801	0.753	2.40	0.401	3.36	0.509	64.8	0.40	2.95
B925	Dolostone	21.0	36.2	3.55	9.95	1.37	0.210	2.54	0.437	2.950	0.788	2.57	0.458	3.61	0.579	86.2	0.34	3.92
B920	Dolostone	0.132	0.206	0.023	0.103	0.029	0.008	0.043	0.007	0.054	0.010	0.048	0.006	0.046	0.007	0.72	0.70	1.92
B03	Pyrite	3.26	13.7	1.58	7.49	1.54	0.328	1.61	0.402	2.58	0.466	1.64	0.225	1.32	0.217	36.4	0.64	1.67
B06	Pyrite	1.12	2.07	0.263	0.884	0.292	0.057	0.142	0.04	0.166	0.028	0.109	0.019	0.072	0.012	5.27	0.86	10.49
B05	Sphalerite	0.069	0.06	0.012	0.085	0.143	0.032	0.018	0.002	0.006	0.002	0.007	0.001	0.004	0.001	0.44	1.93	11.63
B08	Sphalerite	0.208	0.489	0.052	0.226	0.129	0.059	0.077	0.018	0.106	0.014	0.049	0.008	0.059	0.010	1.50	1.81	2.38
B09	Sphalerite	0.353	0.888	0.152	0.922	0.338	0.074	0.170	0.044	0.208	0.043	0.076	0.018	0.087	0.013	3.39	0.94	2.74
B15	Sphalerite	0.082	0.079	0.006	0.149	0.096	0.025	0.009	0.001	0.006	0.003	0.007	0.003	0.017	0.003	0.49	2.60	3.25
B17	Sphalerite	0.049	0.05	0.011	0.125	0.061	0.009	0.003	0.002	0.008	0.003	0.006	0.003	0.013	0.002	0.35	2.03	2.54
B18	Sphalerite	0.291	0.427	0.052	0.224	0.076	0.054	0.044	0.002	0.030	0.004	0.009	0.005	0.016	0.002	1.24	2.86	12.26
B20	Sphalerite	0.003	0.011	0.032	0.123	0.061	0.016	0.011	0.003	0.011	0.005	0.007	0.001	0.005	0.001	0.29	1.89	0.40
B21	Sphalerite	0.189	0.163	0.018	0.139	0.100	0.029	0.013	0.003	0.029	0.004	0.017	0.002	0.019	0.002	0.73	2.46	6.71
B924	Sphalerite	0.255	0.142	0.017	0.107	0.036	0.022	0.023	0.003	0.026	0.004	0.011	0.004	0.021	0.002	0.67	2.34	8.19
B10	Galena	0.202	0.149	0.018	0.088	0.021	0.002	0.017	0.002	0.007	0.002	0.005	0.001	0.005	0.001	0.52	0.32	27.24
B02	Calcite	4.12	10.1	2.01	10.9	4.07	0.601	4.01	0.492	2.61	0.504	1.01	0.087	0.501	0.033	41.1	0.45	5.54
B10	Calcite	2.31	6.54	1.05	6.21	1.98	0.132	1.85	0.201	1.03	0.114	0.373	0.027	0.185	0.031	22.0	0.21	8.42

$\delta Eu = Eu/Eu^* = Eu_N/0.5(Sm_N + Gd_N)$.

Doe, 1981). Additionally, all the sulfides and country whole-rock samples have μ values (Table 4) within the range of crust. All these observations suggest that the Pb of sulfide ores and country rocks in the Banbanqiao deposit area has a crustal source. On the other hand, it is clear that country whole-rock samples have more radiogenic Pb than sulfides (Fig. 8A and B), suggesting that the country rocks are not the main source of Pb in the hydrothermal fluids. Previous studies have indicated that the Proterozoic basement rocks were one of the most important sources in the SYG province (e.g., Zheng and Wang, 1991; Han et al., 2007; Zhou et al., 2013a, 2014a). The Pb isotope data of the Banbanqiao deposit within the range of the basement rocks (Zhou et al., 2014a), so the majority of Pb sourced from the basements.

5.1.4. Implications of rare earth elements

Rare earth elements (REE) aid in determining the origin of the ore-forming elements (e.g., Huston et al., 1995; Huang et al., 2010; Zhou et al., 2011; Souissi et al., 2013). The total REE contents of pyrite and calcite are significantly higher than those of sphalerite and galena (Table 5), and the sulfide ores mainly consists of pyrite, sphalerite, galena and calcite, so the ΣREE of calcite and pyrite can approximatively represent the ΣREE of the hydrothermal fluids (Zhou et al., 2011; Souissi et al., 2013). In the REE chondrite-normalized patterns (Fig. 9), pyrite (Fig. 9C) and calcite (Fig. 9F) samples have similar patterns to those of the hosting dolostone (Fig. 9B), but are different from those of shale (Fig. 9A). This indicates that REE in the hydrothermal solutions were likely to be sourced from the carbonate host rocks. Additionally, the Eu/Eu^* values of pyrite and calcite ($\delta Eu = 0.21–0.86$) are significantly lower than 1, indicating that the hydrothermal fluids were Eu-depleted or derived from Eu-depleted source region. The Liangshan Formation shale whole-rock sample has positive Eu anomaly ($\delta Eu = 2.79$), whereas the Dapu Formation dolostone whole-rock samples have negative Eu anomaly ($\delta Eu = 0.34–0.70$). This also suggests that REE in the ore-forming fluids were likely derived from the carbonate host rocks.

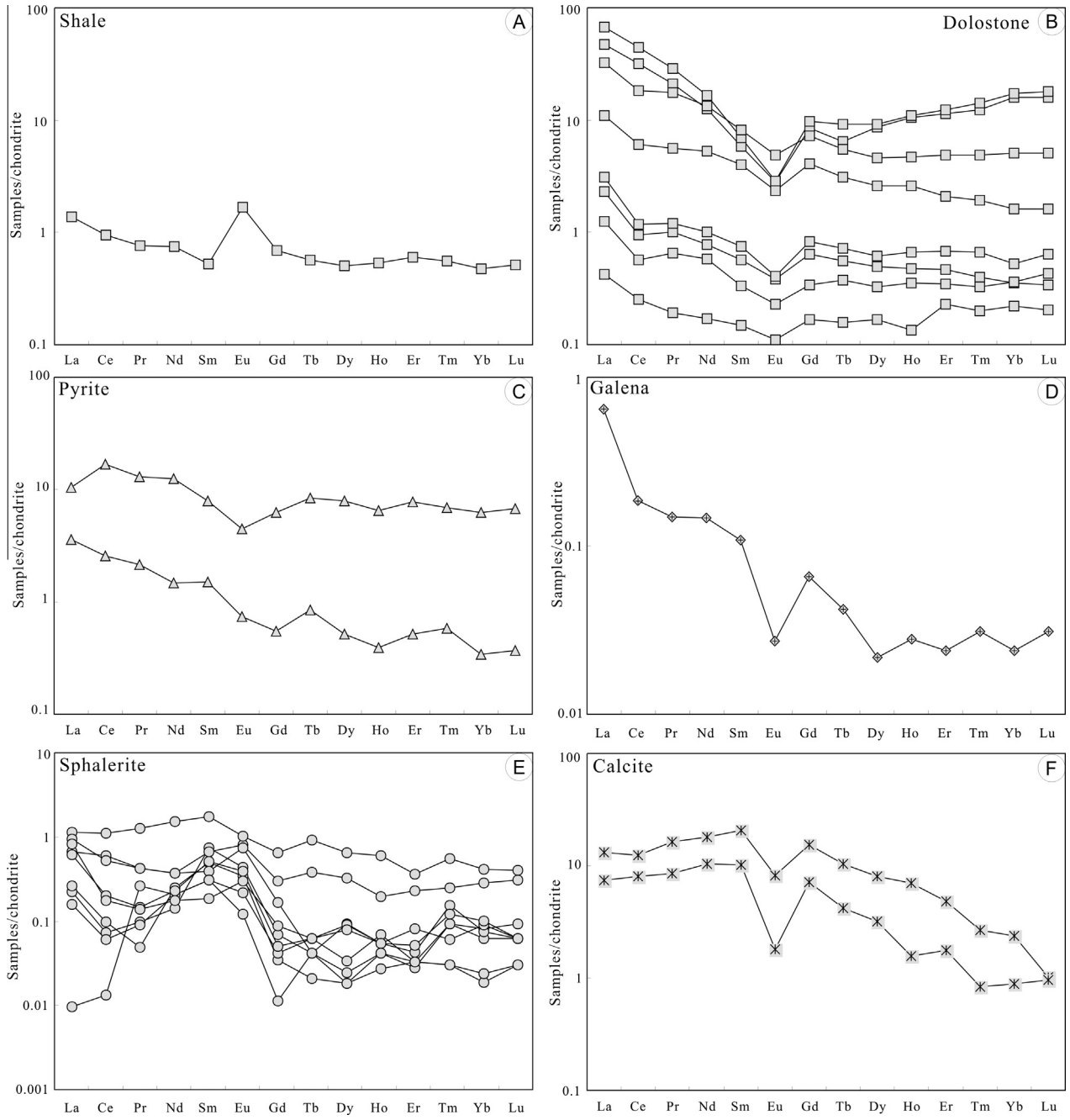

Fig. 9. (A–F) Chondrite-normalized REE patterns (Boynton, 1984). (A) REE pattern for shale. (B) REE patterns for dolostone. (C) REE patterns for pyrite. (D) REE pattern for galena. (E) REE patterns for sphalerite. (F) REE patterns for calcite.

5.2. Ore genesis

Isotope geochronology studies have suggested that the Pb–Zn mineralization in the SYG province occurred during 222–192 Ma in response to the closure of the Paleo-Tethys Ocean (Li et al., 2007b; Lin et al., 2010; Mao et al., 2012; Zhou et al., 2013a,d, 2015; Zhang et al., 2015), which is known as the Indosinian Orogeny (Hu and Zhou, 2012; Zhou et al., 2013a,d; Zhang et al., 2015). These deposits in the western Yangtze Block have been affected by multiple orogenic events after the Indosinian Orogeny (e.g., Zaw et al., 2007; Hu and Zhou, 2012). It is clear that most of these Pb–Zn deposits in the SYG province are epigenetic, but origin of them is complex and cannot easily determined, as suggested by Cd, Ge and Zn isotopes (Fig. 10; Zhu et al., 2013; Zhou et al., 2014a,b; Meng et al., 2015). For example, although the ages (222–192 Ma) of Pb–Zn deposits is much younger than the mantle-derived Emeishan basalts (Ca. ~260 Ma; Zhou et al., 2002b), it has been suggested that the basalts provided ore-forming thermal dynamic and parts of metallogenic materials (such as O and S) for the deposits (Xie, 1963; Huang et al., 2010; Bai et al., 2013; Xu et al., 2014; Zhou et al., 2014a, 2014b; Zhang et al., 2015; Section 5.1). The Pb–Zn deposits in the SYG province can be comparable to typical MVT-type deposits (e.g., Leach et al., 2001, 2005, 2010; Muchez et al., 2005; Oliver, 1986, 1992; Pirajno, 2009, 2013) in terms of geological setting, ore-bearing rocks and source related to basin brine (Zheng and Wang, 1991; Zhou et al., 2001; Wu et al., 2013; Zhang et al., 2015). However, these deposits display a set of characteristics that contrast with

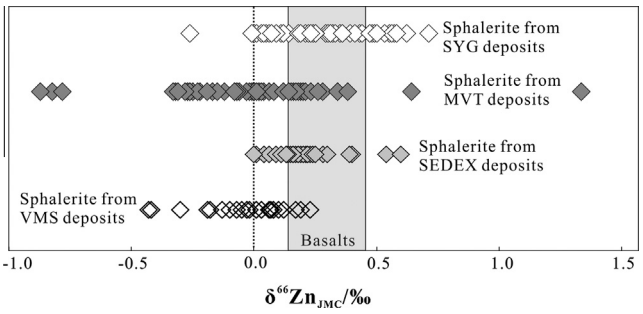

Fig. 10. Comparison of Zn isotopic compositions between sphalerite from SYG deposits and Pb–Zn deposits of MVT, SEDEX and VMS types (after Zhou et al., 2014b).

those of typical MVT-type deposits, including ore-controlled thrust faults and fold structures (convergent geodynamic setting), high grade of Pb + Zn (>15 wt.%), complex sources (carbonate host rocks, Emeishan basalts and basement rocks; see Section 5.1) of ore-forming elements, moderate temperature (150–270 °C), medium to low salinity (<15 wt.% NaCl), weak wall rock alteration and the lack of collapse breccias (e.g., Han et al., 2007; Bai et al., 2013; Zhou et al., 2011, 2013a, 2014b; Xu et al., 2014). Therefore, the Banbanqiao deposit is a carbonate-hosted, stratiform, anticline-controlled, epigenetic and high grade Zn–Pb deposit formed by elemental compositions of mixed origin, and is a typical SYG-type deposit in the western Yangtze Block, southwest China (Zhou et al., 2013a, 2014b, 2015). The mineralization process is similar to that of brine-related deposits elsewhere, including extraction of ore-forming elements from all kinds of rocks by convective circulation of hydrothermal fluids, and then they mixed with sulfate ion- and organic matter-bearing cool water and subsequent reduction of SO_4^{2-} to S^{2-} and precipitation of these elements in favorable structural and lithological units (Hu and Zhou, 2012; Zhou et al., 2014b).

6. Conclusions

Ore bodies in the Banbanqiao deposit occur within axis of NNE-trending Banbanqiao anticline. C–O–S–Pb isotopes and REE suggest: (i) C in the hydrothermal fluids was the dissolved product of the carbonate host rocks, (ii) O in the ore-forming fluids was derived from a mixed source of mantle-derived O in Emeishan basalts and dissolved O from the carbonate host rocks, (iii) S in the ore-forming solutions was sourced from evaporites by TSR with a limited influence of mantle-derived S, (iv) Pb in the hydrothermal fluids was originated from a mixed source of the basement rocks and the carbonate host rocks, and (v) REE in the hydrothermal fluids were sourced from the carbonate host rocks. The fluids' mixing is an important mechanism for the Banbanqiao sulfide formation. Ore genesis of the Banbanqiao deposit is different from the typical MVT-type deposit, it is a carbonate-hosted, stratiform, anticline-controlled, epigenetic and high grade Zn–Pb deposit formed by elemental compositions of mixed origin, and is a typical SYG-type deposit.

Acknowledgements

This research was financially supported jointly by the National Basic Research Program of China (No. 2014CB440905), the Key Program of National Natural Science Foundation of China (No. 41430315) and the National Natural Science Foundation of China (Nos. 41163001, 41272111 and 41402072). Thanks are given to Prof. Mei-Fu Zhou and Dr. Xiao-Chun Li for useful discussion and modification. Comments and suggestions from Prof. Bor-ming Jahn (Editor-in-Chief), Miss Irene Yao and two anonymous reviewers have greatly enhanced the paper.

References

Badrzadeh, Z., Barrett, T.J., Peter, J.M., Gimeno, D., Sabzehei, M., Aghazadeh, M., 2011. Geology, mineralogy, and sulfur isotope geochemistry of the Sargaz Cu–Zn volcanogenic massive sulfide deposit, Sanandaj-Sirjan Zone. Iran. Miner. Deposita 46, 905–923.

Bai, J.H., Huang, Z.L., Zhu, D., Yan, Z.F., Zhou, J.X., 2013. Isotopic compositions of sulfur in the Jinshachang lead–zinc deposit, Yunnan, China. Acta Geol. Sin. (Engl. Ed.) 87, 1355–1369.

Basuki, N.I., Taylor, B.E., Spooner, E.T.C., 2008. Sulfur isotope evidence for thermochemical reduction of dissolved sulfate in Mississippi valley type zinc–lead mineralization, Bongara area, northern Peru. Econ. Geol. 103, 183–799.

Boynton, W.V., 1984. Cosmochemistry of the rare earth elements: meteorite studies. In: Henderson, P. (Ed.), Rare Earth Element Geochemistry. Elsevier, Amsterdam, pp. 63–114.

Carr, G.R., Dean, J.A., Suppel, D.W., Heithersay, P.S., 1995. Precise lead isotope fingerprinting of hydrothermal activity associated with Ordovician to Carboniferous metallogenic events in the Lachlan fold belt of New South Wales. Econ. Geol. 90, 1467–1505.

Chaussidon, M., Albarède, F., Sheppard, S.M.F., 1989. Sulphur isotope variations in the mantle from ion microprobe analyses of micro-sulphide inclusions. Earth Planet. Sci. Lett. 92, 144–156.

Chen, S.J., 1986. A discussion on the sedimentary origin of Pb–Zn deposits in western Guizhou and northeastern Yunnan. Guizhou Geol. 8, 35–39 (in Chinese with English abstract).

Chung, S.L., Jahn, B.M., 1995. Plume–lithosphere interaction in generation of the Emeishan flood basalts at the Permian-Triassic boundary. Geology 23, 889–892.

Claypool, G.E., Holser, W.T., Kaplan, I.R., Sakai, H., Zak, I., 1980. The age curves of sulfur and oxygen isotopes in marine sulfate and their mutual interpretation. Chem. Geol. 28, 199–260.

Cromie, P.W., Gosse, R.R., Zhang, P., Zhu, X., 1996. Exploration for carbonate-hosted Pb–Zn deposits, Sichuan, P.R.C. [abs.]: International Geological Congress, 30th, Beijing, China, p. 412 (Abstracts).

Czamanske, G.K., Rye, R.O., 1974. Experimentally determined sulfur isotope fractionations between sphalerite and galena in the temperature range 600 C to 275 C. Econ. Geol. 69, 17–25.

Demény, A., Ahijado, A., Casillas, R., Vennemann, T.W., 1998. Crustal contamination and fluid/rock interaction in the carbonatites of Fuerteventura (Canary Islands, Spain): a C, O, H isotope study. Lithos 44, 101–115.

Demény, A., Harangi, S.Z., 1996. Stable isotope studies on carbonate formations in alkaline basalt and lamprophyre series: evolution of magmatic fluids and magma–sediment interactions. Lithos 37, 335–349.

Deng, H.L., Li, C.Y., Tu, G.Z., Zhou, Y.M., Wang, C.W., 2000. Strontium isotope geochemistry of the Lemachang independent silver ore deposit, northeastern Yunnan, China. Sci. China: Earth Sci. 43, 337–346.

Dixon, G., Davidson, G.J., 1996. Stable isotope evidence for thermo-chemical sulfate reduction in the Dugald River (Australia) strata-bound shale-hosted zinc–lead deposit. Chem. Geol. 129, 227–246.

Friedman, I., O'Neil, J.R., 1977. Compilation of Stable Isotope Fractionation Factors of Geochemical Interest. Data of Geochemistry, U.S. Geological Survey Professional Paper 440-KK, p. 1–12.

Han, R.S., Liu, C.Q., Huang, Z.L., Chen, J., Ma, D.Y., Lei, L., Ma, G.S., 2007. Geological features and origin of the Huize carbonate-hosted Zn–Pb–(Ag) District, Yunnan, South China. Ore Geol. Rev. 31, 360–383.

Hu, R.Z., Zhou, M.F., 2012. Multiple Mesozoic mineralization events in South China – an introduction to the thematic issue. Miner. Deposita 47, 579–588.

Huang, Z.L., Li, W.B., Chen, J., Han, R.S., Liu, C.Q., Xu, C., Guan, T., 2003. Carbon and Oxygen isotope constraints on the mantle fluids join the mineralization of the Huize super-large Pb–Zn deposits, Yunnan Province, China. J. Geochem. Explor. 78 (79), 637–642.

Huang, Z.L., Li, X.B., Zhou, M.F., Li, W.B., Jin, Z.G., 2010. REE and C–O isotopic geochemistry of calcites from the world-class Huize Pb–Zn deposit, Yunan, China: implications for the ore genesis. Acta Geol. Sin. (Engl. Ed.) 84, 597–613.

Huston, D.L., Sie, S.H., Suter, G.F., Cooke, D.R., Both, R.A., 1995. Trace elements in sulfide minerals from Eastern Australian volcanic-hosted massive sulfide deposits: Part 1. Proton microprobe analyses of pyrite, chalcopyrite, and sphalerite, and Part 2. Selenium levels in pyrite: Comparison with $\delta^{34}S$ values and implications for the source of sulfur in volcanogenic hydrothermal systems. Econ. Geol. 90, 1167–1196.

Leach, D.L., Bradley, D.C., Huston, D., Pisarevsky, S.A., Taylor, R.D., Gardoll, S.J., 2010. Sediment-hosted lead–zinc deposits in Earth history. Econ. Geol. 105, 593–625.

Leach, D.L., Sangster, D., Kelley, K.D., Large, R.R., Garven, G., Allen, C., Gutzmer, J., Walters, S., 2005. Sediment-hosted lead–zinc deposits: a global perspective. Econ. Geol. 100th Anniversary, 561–607.

Leach, D.L., Bradley, D., Lewchuk, M.T., Symons, D.T., de Marsily, G., Brannon, J., 2001. Mississippi Valley-type lead–zinc deposits through geological time: implications from recent age-dating research. Miner. Deposita 36, 711–740.

Li, W.B., Huang, Z.L., Yin, M.D., 2007a. Isotope geochemistry of the Huize Zn–Pb ore field, Yunnan province, southwestern China: implication for the sources of ore fluid and metals. Geochem. J. 41, 65–81.
Li, W.B., Huang, Z.L., Yin, M.D., 2007b. Dating of the giant Huize Zn–Pb ore field of Yunnan province, southwest China: Constrains from the Sm–Nd system in hydrothermal calcite. Resour. Geol. 57, 90–97.
Lin, Z.Y., Wang, D.H., Zhang, C.Q., 2010. Rb–Sr isotopic age of sphalerite from the Paoma lead–zinc deposit in Sichuan Province and its implications. Geol. China 37, 488-196, (in Chinese with English abstract).
Liu, H.C., Lin, W.D., 1999. Study on the law of Pb–Zn–Ag ore deposits in Northeast Yunnan, China. Yunnan University Press, Kunming, pp. 1–468 (in Chinese with English abstract).
Liu, J.M., Liu, J.J., 1997. Basin fluid genetic model of sediment-hosted micro-disseminated gold deposits in the gold-triangle area between Guizhou, Guangxi and Yunnan. Acta Mineral. Sin. 17, 448–456 (in Chinese with English abstract).
Mao, J.W., Zhou, Z.H., Feng, C.Y., Wang, Y.T., Zhang, C.Q., Peng, H.J., Yu, M., 2012. A preliminary study of the Triassic large-scale mineralization in China and its geodynamic setting. Geol. China 39, 1437–1471 (in Chinese with English abstract).
Meng, Y.M., Qi, H.W., Hu, R.Z., 2015. Determination of germanium isotopic compositions of sulfides by hydride generation MC-ICP-MS and its application to the Pb–Zn deposits in SW China. Ore Geol. Rev. 65, 1095–1109.
Muchez, P., Heijlen, W., Banks, D., Blundell, D., Boni, M., Grandia, F., 2005. Extensional tectonics and the timing and formation of basin-hosted deposits in Europe. Ore Geol. Rev. 27, 241–267.
Ohmoto, H., Kaiser, C.J., Geer, K.A., 1990. Systematics of sulphur isotopes in recent marine sediments and ancient sediment-hosted base metal deposits. In: Herbert, H.K., Ho, S.E. (Eds.), Stable Isotopes and Fluid Processes in Mineralization. Geol Dep Univ Extens Univ Western Australia, 23, pp. 70–120.
Ohmoto, H., 1972. Systematics of sulfur and carbon isotopes in hydrothermal ore deposits. Econ. Geol. 67, 551–579.
Ohmoto, H., Goldhaber, M.B., 1997. Sulfur and carbon isotopes. In: Barnes, H.L. (Ed.), Geochemistry of Hydrothermal Ore Deposits, third ed. Wiley, New York, pp. 517–611.
Oliver, J., 1986. Fluids expelled tectonically from orogenic belts: their role in hydrocarbon migration and other geologic phenomena. Geology 14, 99–102.
Oliver, J., 1992. The spots and stains of plate tectonics. Earth-Sci. Rev. 32, 77–106.
Palinkaš, S.S., Palinkaš, L.A., Renac, C., Spangenberg, J.E., Lüders, V., Molnar, F., Maliqi, G., 2013. Metallogenic model of the Trepča Pb–Zn–Ag skarn deposit, Kosovo: evidence from fluid inclusions, rare earth elements, and stable isotope data. Econ. Geol. 108, 135–162.
Pass, H.E., Cooke, D.R., Davidson, G., Maas, R., Dipple, G., Rees, C., Ferreira, L., Taylor, C., Deyell, C.L., 2014. Isotope geochemistry of the northeast zone, Mount Polley alkalic Cu–Au–Ag porphyry deposit, British Columbia: a case for carbonate assimilation. Econ. Geol. 109, 859–890.
Pirajno, F., 2009. Hydrothermal Processes and Mineral Systems. Springer, Berlin, pp. 1256.
Pirajno, F., 2013. The Geology and Tectonic Setting of China's Mineral Deposits. Springer, Berlin, pp. 123–183.
Qi, L., Hu, J., Gregoire, D.C., 2000. Determination of trace elements in granites by inductively coupled plasma mass spectrometry. Talanta 51, 507–513.
Qiu, Y.M., Gao, S., McNaughton, N.J., Groves, D.I., Ling, W.L., 2000. First evidence of >3.2 Ga continental crust in the Yangtze craton of south China and its implications for Archean crustal evolution and Phanerozoic tectonics. Geology 28, 11–14.
Reid, A., Wilson, C.J.L., Shun, L., Pearson, N., Belousova, E., 2007. Mesozoic plutons of the Yidun Arc, SW China: U/Pb geochronology and Hf isotopic signature. Ore Geol. Rev. 31, 88–106.
Seal, I.R., 2006. Sulfur isotope geochemistry of sulfide minerals. Rev. Mineral. Geochem. 61, 633–677.
Souissi, F., Jemmali, N., Souissi, R., Dandurand, J.L., 2013. REE and isotope (Sr, S and Pb) geochemistry to constrain the genesis and timing of the F–(Ba–Pb–Zn) ores of the Zaghouan District (NE Tunisia). Ore Geol. Rev. 55, 1–12.
Sun, W.H., Zhou, M.F., Gao, J.F., Yang, Y.H., Zhao, X.F., Zhao, J.H., 2009. Detrital zircon U–Pb geochronological and Lu–Hf isotopic constraints on the Precambrian magmatic and crustal evolution of the western Yangtze Block, SW China. Precambr. Res. 172, 99–126.
Taylor, J.H.P., Frechen, J., Degens, E.T., 1967. Oxygen and carbon isotope studies of carbonatites from the Laacher See District, West Germany and the Alno District Sweden. Geochim. Cosmochim. Acta 31, 407–430.
Veizer, J., Hoefs, J., 1976. The nature of $^{18}O/^{16}O$ and $^{13}C/^{12}C$ secular trends in sedimentary carbonate rocks. Geochim. Cosmochim. Acta 40, 1387–1395.
Wu, Y., Zhang, C.Q., Mao, J.W., Ouyang, H.G., Sun, J., 2013. The genetic relationship between hydrocarbon systems and Mississippi Valley-type Zn–Pb deposits along the SW margin of Sichuan Basin, China. Int. Geol. Rev. 55, 941–957.
Xie, J.R., 1963. Introduction of the Chinese ore Deposits. Science Press, Beijing, pp. 1–71 (in Chinese).
Xu, Y.K., Huang, Z.L., Zhu, D., Luo, T.Y., 2014. Origin of hydrothermal deposits related to the Emeishan magmatism. Ore Geol. Rev. 63, 1–8.
Yan, D.P., Zhou, M.F., Song, H.L., Wang, X.W., Malpas, J., 2003. Origin and tectonic significance of a Mesozoic multi-layer over-thrust system within the Yangtze Block (South China). Tectonophysics 361, 239–254.
Ye, L., Cook, N.J., Ciobanu, C.L., Liu, Y.P., Zhang, Q., Liu, T.G., Gao, W., Yang, Y.L., Danyushevsky, L., 2011. Trace and minor elements in sphalerite from base metal deposits in South China: a LA-ICPMS study. Ore Geol. Rev. 39, 188–217.
Zartman, R.E., Doe, B.R., 1981. Plumbotectonics – the model. Tectonophysics 75, 135–162.
Zaw, K., Peters, S.G., Cromie, P., Burrett, C., Hou, Z., 2007. Nature, diversity of deposit types and metallogenic relations of South China. Ore Geol. Rev. 31, 3–47.
Zhao, X.F., Zhou, M.F., Li, J.W., Sun, M., Gao, J.F., Sun, W.H., Yang, J.H., 2010. Late Paleoproterozoic to early Mesoproterozoic Dongchuan Group in Yunnan, SW China: implications for tectonic evolution of the Yangtze Block. Precambr. Res. 182, 57–69.
Zhang, C.Q., Wu, Y., Hou, L., Mao, J.W., 2015. Geodynamic setting of mineralization of Mississippi Valley-type deposits in world-class Sichuan–Yunnan–Guizhou Zn–Pb triangle, southwest China: implications from age-dating studies in the past decade and the Sm–Nd age of the Jinshachang deposit. J. Asian Earth Sci. 103, 103–114.
Zheng, M.H., Wang, X.C., 1991. Genesis of the Daliangzi Pb–Zn deposit in Sichuan, China. Econ. Geol. 86, 831–846.
Zheng, Y.F., Chen, J.F., 2000. Stable Isotope Geochemistry. Science Press, Beijing, pp. 10–50 (in Chinese).
Zhou, C.X., Wei, C.S., Guo, J.Y., 2001. The source of metals in the Qilingchang Pb–Zn deposit, Northeastern Yunnan, China: Pb–Sr isotope constraints. Econ. Geol. 96, 583–598.
Zhou, J.X., Huang, Z.L., Zhou, G.F., Li, X.B., Ding, W., Bao, G.P., 2011. Trace elements and rare earth elements of sulfide minerals in the Tianqiao Pb–Zn Ore deposit, Guizhou Province, China. Acta Geol. Sin. (Engl. Ed.) 85, 189–199.
Zhou, J.X., Huang, Z.L., Zhou, M.F., Li, X.B., Jin, Z.G., 2013a. Constraints of C–O–S–Pb isotope compositions and Rb–Sr isotopic age on the origin of the Tianqiao carbonate-hosted Pb–Zn deposit, SW China. Ore Geol. Rev. 53, 77–92.
Zhou, J.X., Huang, Z.L., Bao, G.P., 2013b. Geological and sulfur–lead–strontium isotopic studies of the Shaojiwan Pb–Zn deposit, southwest China: Implications for the origin of hydrothermal fluids. J. Geochem. Explor. 128, 51–61.
Zhou, J.X., Huang, Z.L., Gao, J.G., Yan, Z.F., 2013c. Geological and C–O–S–Pb–Sr isotopic constraints on the origin of the Qingshan carbonate-hosted Pb–Zn deposit, SW China. Int. Geol. Rev. 55, 904–916.
Zhou, J.X., Huang, Z.L., Yan, Z.F., 2013d. The origin of the Maozu carbonate-hosted Pb–Zn deposit, southwest China: constrained by C–O–S–Pb isotopic compositions and Sm–Nd isotopic age. J. Asian Earth Sci. 73, 39–47.
Zhou, J.X., Huang, Z.L., Bao, G.P., Gao, J.G., 2013e. Sources and thermo-chemical sulfate reduction for reduced sulfur in the hydrothermal fluids, southeastern SYG Pb–Zn metallogenic province, SW China. J. Earth Sci. 24, 759–771.
Zhou, J.X., Huang, Z.L., Zhou, M.F., Zhu, X.K., Muchez, P., 2014a. Zinc, sulfur and lead isotopic variations in carbonate-hosted Pb–Zn sulfide deposits, southwest China. Ore Geol. Rev. 58, 41–54.
Zhou, J.X., Huang, Z.L., Lv, Z.C., Zhu, X.K., Gao, J.G., Mirnejad, H., 2014b. Geology, isotope geochemistry and ore genesis of the Shanshulin carbonate-hosted Pb–Zn deposit, southwest China. Ore Geol. Rev. 63, 209–225.
Zhou, J.X., Bai, J.H., Huang, Z.L., Zhu, D., Yan, Z.F., Lv, Z.C., 2015. Geology, isotope geochemistry and geochronology of the Jinshachang carbonate-hosted Pb–Zn deposit, South China. J. Asian Earth Sci. 98, 272–284.
Zhou, M.F., Yan, D.P., Kennedy, A.K., Li, Y.Q., Ding, J., 2002a. SHRIMP zircon geochronological and geochemical evidence for Neo-proterozoic arc-related magmatism along the western margin of the Yangtze Block, South China. Earth Planet. Sci. Lett. 196, 1–67.
Zhou, M.F., Malpas, J., Song, X.Y., Kennedy, A.K., Robinson, P.T., Sun, M., Lesher, M., Keays, R.R., 2002b. A temporal link between the Emeishan large igneous province (SW China) and the end-Guadalupian mass extinction. Earth Planet. Sci. Lett. 196, 113–122.
Zhu, C.W., Wen, H.J., Zhang, Y.X., Fan, H.F., Fu, S.H., Xu, J., Qin, T.R., 2013. Characteristics of Cd isotopic compositions and their genetic significance in the lead–zinc deposits of SW China. Sci. China: Earth Sci. 56, 2056–2065.